ARTICLE

doi:10.1038/nature19332

Perimortem fractures in Lucy suggest mortality from fall out of tall tree

John Kappelman[1,2], Richard A. Ketcham[2], Stephen Pearce[3], Lawrence Todd[1], Wiley Akins[4], Matthew W. Colbert[2], Mulugeta Feseha[5], Jessica A. Maisano[2] & Adrienne Witzel[1]

The Pliocene fossil 'Lucy' (*Australopithecus afarensis*) was discovered in the Afar region of Ethiopia in 1974 and is among the oldest and most complete fossil hominin skeletons discovered. Here we propose, on the basis of close study of her skeleton, that her cause of death was a vertical deceleration event or impact following a fall from considerable height that produced compressive and hinge (greenstick) fractures in multiple skeletal elements. Impacts that are so severe as to cause concomitant fractures usually also damage internal organs; together, these injuries are hypothesized to have caused her death. Lucy has been at the centre of a vigorous debate about the role, if any, of arboreal locomotion in early human evolution. It is therefore ironic that her death can be attributed to injuries resulting from a fall, probably out of a tall tree, thus offering unusual evidence for the presence of arborealism in this species.

It is rare when an early hominin fossil composed of multiple skeletal elements representing a single individual is discovered[1–5], and rarer still when a cause of death can potentially be attributed to its remains[6,7]. A.L. 288-1, named Lucy and dated to 3.18 million years in age[8], is represented by elements of the skull, upper limb, hand, axial skeleton, pelvis, lower limb, and foot, with some bilateral preservation (Fig. 1a), and is popularly described as 40% complete[9]. We studied the original fossil and computed tomographic (CT) scans of the skeleton to assess cause of death. Our observation that the skeleton is marked by post-mortem damage largely agrees with the original description[9]; however, we differ from the original authors in proposing that a subset of fractures are likely to be perimortem and were produced by a vertical deceleration event, or a fall and impact from considerable height, and not by fossilization processes.

Perimortem compressive fractures

The most striking feature of the nearly complete right humerus (A.L. 288-1m) is that its proximal end is severely damaged[9] (Fig. 1b, c). Close examination shows that it underwent severe valgus head-shattering compression that drove the head fragments into the shaft, fracturing the greater and lesser tuberosities, and fracturing and dislocating a portion of the proximal shaft with the intertubercular groove (Fig. 1b, bottom). The shaft of the right humerus was found as multiple segments with generally tight fits. The two major segments conjoin near the midshaft, where a fragment of displaced cortical bone reveals that the shaft underwent a spiral fracture that operated in the same direction as the compressive fracture at the head (Fig. 1b, d, Supplementary Note 1, and Extended Data Figs 1, 2).

Lucy's right scapula (A.L. 288-1l) was found as three pieces with the major fragment preserving a complete and undamaged glenoid and neck along with a portion of the base of the coracoid process; the other two fragments preserve a short portion of the lateral border and the base of the acromion. This pattern matches that of the most common fractures of the scapula[10].

A fracture of the articular head, lesser tuberosity, greater tuberosity, and shaft of the humerus is classified as a four-part proximal humerus fracture[11]. Under natural conditions, this fracture is commonly caused by an impact following a vertical deceleration event when an accident victim consciously stretches out their arm in an attempt to break their fall. Compressive contact between the hand and the ground impacts the humeral articular head against the glenoid which, with the glenoid acting as anvil[12], fractures some or all of the components of the proximal humerus. This fracture leaves a unique signature on the humeral head and is common in two distinct populations: elderly people who have suffered a reduction in bone strength when even a fall from standing height onto an outstretched arm can fracture and sometimes compress the head into the greatly weakened shaft; and people with healthy bone strength who experience a fall from considerable height that in turn produces an impact with more powerful forces acting on the outstretched arm[13]. A 3D reconstruction of the right humerus based on CT data illustrates how Lucy's articular head and shaft were compressively fractured (Supplementary Note 2 and Supplementary Video 1).

Lucy's left proximal humerus (A.L. 288-1r) is largely complete but damage at the head reveals that it too suffered a compressive fracture (Fig. 1e). The general pattern is similar to that seen in the much more extensively fractured right humerus but it is less severely damaged (Supplementary Note 1).

These humeral fractures were long thought to have occurred post-mortem, but their close match to clinical cases[11–13] (Table 1) suggests instead that they represent perimortem injuries. The fracture edges are sharp and clean, and bone fragments along with tiny bone slivers (<1 mm) of the severely shattered right articular head and shaft (Fig. 1b–d and Extended Data Figs 1, 2) and left proximal humerus (Fig. 1e) are preserved in their post-injury positions. This evidence suggests that the compressive impact event occurred while the periosteum and joint capsule were intact; if these factures had occurred after the periosteum and joint capsule had decomposed and when the bone was dry, it is likely that the slivers and fragments would have been dispersed onto the surface of the ground or into the soil. Additional evidence for perimortem fractures is found in the fact that there is no evidence of healing along any of these sharp fracture edges (Supplementary Note 3). Although compressive bilateral proximal humerus fractures are not common, under natural conditions these

[1]Department of Anthropology, The University of Texas at Austin, Austin, Texas 78712, USA. [2]Department of Geological Sciences, The University of Texas at Austin, Austin, Texas 78712, USA. [3]Austin Bone and Joint Clinic, Austin, Texas 78705, USA. [4]Department of Radio-Television-Film, The University of Texas at Austin, Austin, Texas 78712, USA. [5]Paleoanthropology and Paleoenvironment Program, Addis Ababa University, Addis Ababa, Ethiopia.

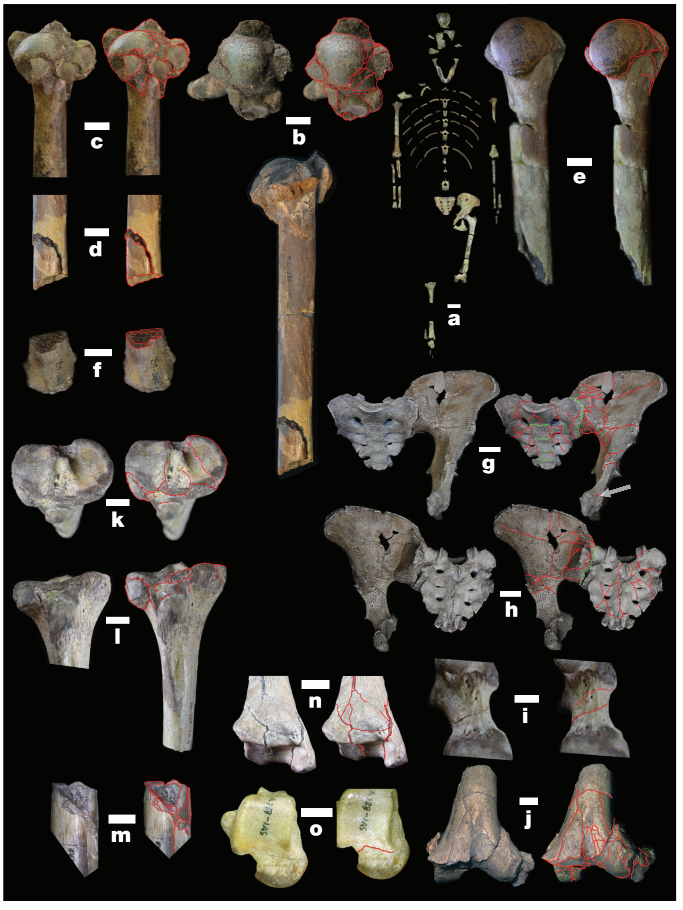

Figure 1 | Perimortem fractures in A.L. 288-1 postcranial skeleton consistent with vertical deceleration event. a, Lucy. **b**, **c**, Right humerus (**b**, top: stereo, superior, medial up; bottom: lateral; **c**, stereo, posterior) preserves valgus head-shattering four-part proximal fracture. **d**, Hinge and spiral fracture elevated, displaced, and fractured right midshaft humeral bone fragment (stereo, lateral; see **b**). **e**, Head of left humerus (stereo, medial) is fractured and compressed inferomedially to override the neck. **f**, Fracture of right distal radius (posterior, stereo view). **g**, Fractures in sacrum (stereo, anterior) and left innominate just lateral to sacrum. Fractured superior pubic ramus also visible as is puncture hole (arrow). **h**, Left-lateral asymmetry of fractured sacrum (stereo, posterior) and fractured, elevated, and bent retroauricular surface of left innominate. **i**, Left femoral neck fractures (stereo, lateral at top). **j**, Superoposteriorly fractured epiphysis of left distal femur (stereo, anterior) in discovery state with lateral extent sheared superiorly along lateral edge of shaft. Central portion of anterodistal shaft fractured and secondarily driven into trabeculae. **k**, Fracture of right tibial plateau (stereo, superior, medial to right) with major fracture across medial condyle that with other fractures (**l**; stereo, anterior, medial to right) depress the plateau and add valgus cant to shaft. **m**, Proximal portion of right distal tibia (stereo, posteromedial, superior at top) preserves small bone fragments broken loose and driven into medullary canal at spiral shaft fracture. **n**, Fractures on talar articular surface of right distal tibia (stereo, anterior, medial to right) open onto anterodistal surface of shaft. **o**, Right talus neck fracture (stereo, superior, medial to right). Together, **n** and **o** are consistent with a pilon fracture. Red lines are fractures; green lines in **g**, **h** denote sacroiliac joint and transverse lines of sacrum. Specimens in **g** and **h** are casts because it was not practical to articulate the fossils, and **j** is a cast because the original specimen was reconstructed. Scale bars (**a**, 50 mm; **b**–**f**, **i**–**o**, 10 mm; **g**, **h**, 20 mm) are approximate, given stereo photo parallax. See Extended Data Figs 1–4, Supplementary Note 1, and Supplementary Videos 1–4.

fractures are usually associated with high energy trauma resulting from an impact on outstretched arms[14]. The fact that these fractures commonly occur when an accident victim actively abducts and stretches out their arms in an attempt to break their fall suggests that Lucy was conscious at the time of impact, offering additional support to the hypothesis that this was a perimortem event, with Lucy suffering a more severe impact on her right side.

Table 1 | Fractures in Lucy's skeleton consistent with a vertical deceleration event

Element	Side	Description
Humerus	R	Four-part compressive proximal humerus fracture
	R	Hinge and spiral fracture of shaft
	L	Compressive fracture of the proximal humerus head and tuberosities
Scapula	R	Fracture of border and acromion (glenoid undamaged; body not recovered but presumed fractured)
Radius	R	Distal shaft fracture (Colles or Smith)
Pelvis		Left innominate: sacroiliac joint and retroauricular fracture and displacement
		Left innominate: fracture along medial anterior surface
		Left superior and inferior pubic rami: fractures and lateral offset of inferior ramus
		Sacrum: fractures in central elements, R and L lateral mass, and alae
Femur	L	Basicervical and transcervical fractures of the neck
	L	Dislocation and compressive impact of distal epiphysis into distal shaft; compressive fractures of lateral and medial condyles; fracture shear of lateral condyle and epicondyle along lateral side of shaft
	L	Compressive fracture of distal anterior central shaft into trabeculae
Tibia	R	Tibial plateau fracture (elements retained together)
	R	Spiral fracture of diaphysis
	R	Pilon fracture of the distal tibia, type AO-43C (elements retained together)
Talus	R	Talar neck type I non-displaced fracture associated with pilon fracture
Fibula	R	Fracture of distal shaft associated with pilon fracture
Cranium		Fractures of multiple cranial elements (some hinge)
Mandible		Guardsman tripartite fracture (parasymphysis and bilateral subcondylar fractures)
		Bilateral coronoid process fracture (processes missing)
		Left body fracture
Ribs	R	Hinge and midbody fractures of first rib
	R & L	Fractures (some hinge) of multiple individual ribs
Clavicle	R	Fracture of lateral third of shaft
Lumbar vertebra		Vertical fractures in body, fractures of neural arch

The presence of bilateral proximal humerus fractures leads us to hypothesize that some of the other compressive fractures in Lucy's skeleton, and especially those at major joints, also occurred perimortem and can be attributed to a severe impact. Compressive fractures in the left femur (A.L. 288-1ap) are especially informative (Supplementary Note 1). There are two subparallel fractures in the neck oriented in a roughly parasagittal plane (Fig. 1i). The basicervical (narrower) and transcervical (wider) fractures are both widest in their superior aspect and wrap anteriorly and posteriorly around the neck to terminate inferiorly, slightly offsetting the head in an inferior direction. The location and orientation of these fractures suggest that when the pelvis and femur were articulated, a compressive force acted at the hip to drive the acetabulum and femoral head against one another, thereby fracturing the neck.

The fractured fragments of the distal left femur (Fig. 1j) were separated from one another to reconstruct this element, so the following description is based on a cast of the bone in its discovery state (Supplementary Note 1). This region was severely compressively fractured. The articular surface of the lateral condyle was shattered with the dislocated fragments forming a step along its lateral edge, while large cracks (subsequently closed in the reconstruction) separated fragments of the medial condyle's fractured articular surface. The entire femoral epiphysis was separated and compressively driven into the distal shaft in a superoposterior direction. The shaft overrides the superior articular surface of medial condyle, the superior edge of the patellar surface, and the superior extent of the articular surface of the lateral condyle, with the lateral condyle and epicondyle and a portion of the lateral shaft also fractured and compressively sheared superolaterally along the edge of the shaft. The extent of shaft override and lateral shear is apparent in Fig. 1j and especially in the left image of the stereo pair, where the shadow cast by the fractured edge can be seen around the anterodistal circumference of the shaft.

The compressive fractures at both the femoral neck and distal femur appear to have occurred perimortem when the foot impacted the ground following a fall, with the force acting along the long axis of the leg. We hypothesize that the tibial plateau acted as a punch when it impacted the epiphysis, in a manner similar to how the glenoid acted as an anvil at the proximal humerus. Although no left tibia was recovered, we tested this idea by articulating the femoral epiphysis with a 3D printout of Lucy's right proximal tibia (A.L. 288-1aq) mirrored as a left, and the shape of the tibial plateau matches both the contour and dimensions of the indentation preserved on the epiphysis and shows a twist to the right (Supplementary Note 1). The superoposterior orientation of the dislocated epiphysis suggests that the leg was hyperextended during impact. The impact also apparently produced the fractures in the femoral neck. The femoral fragments, and especially the small condylar fragments, remain in their original fractured positions and have sharp, clean edges that show no evidence of healing. As suggested for the humeri, if this fracture had occurred post-mortem on dry bone after the joint capsule and periosteum had decayed, it seems likely that the small fragments would have been dispersed onto the surface of the ground or into the soil. Together, these observations offer additional support for the hypothesis that these compressive fractures occurred perimortem while the tibia and femur were articulated and the joint capsule and periosteum intact. Although no left tibia was recovered, fractures in Lucy's right tibia (Table 1, Fig. 1k–n, and Supplementary Note 1) are consistent with an impact following a fall from height and we propose that the left tibia would be in a similar condition if it were to be discovered.

Additional compressive and hinge (greenstick) fractures are preserved in the forearms, lower limbs, pelvis, thorax (including the rarely fractured first rib), and skull (Fig. 1, Supplementary Note 1, Table 1, Extended Data Figs 3, 4, and Supplementary Videos 2, 3). As seen with the humeri and femur, small bone fragments with sharp, clean edges and no evidence of healing often remain in their original fractured positions, again suggesting that these fractures occurred perimortem. The pattern is consistent with clinical presentations of fractures produced by a severe impact following a fall.

Mechanisms of bone fracture

There are other mechanisms, in addition to vertical deceleration events, that can fracture bone; these include collisions between a body and moving or stationary objects during floods, violent contact with animals, and even tetanic muscle contractions produced by seizures or lightning strikes (Supplementary Note 4). However, these other mechanisms are uncommon and do not generally produce fractures by compression along the long axis of the bone (although some of these latter mechanisms can cause a fall that in turn generates compressive fractures). Lucy's fractures most closely resemble and are consistent with those seen in patients who have suffered a vertical deceleration event from considerable height that in turn produces concomitant fractures across the skeleton[15–18].

Hadar palaeohabitats and inferred tree use

Given this combination of evidence, the question remains as to how Lucy could have achieved the height necessary to produce the high velocity fall and impact required to fracture her skeleton so severely. One of the most vigorously debated questions in palaeoanthropology has been the role, if any, of arboreal locomotion in early hominin evolution and especially in Lucy's species, *Australopithecus afarensis*[19], which demonstrates convincing adaptations to terrestrial bipedalism. Given Lucy's small size, she, like many small primates, probably sought nightly refuge in trees[20] and possibly foraged there, so it is reasonable to assess whether trees were available to her. Palaeohabitat reconstructions based on fossil mammals[21], fossil pollen[22], and palaeopedology and $\delta^{18}O$ and $\delta^{13}C$ analysis of palaeosol carbonates[23] have led to the conclusion that Hadar, where Lucy was found, was a grassy woodland with sizable trees. Lucy was found in a sandstone deposited as a distributary crevasse-splay channel over a low-relief area of the floodplain[24]; this shallow channel was probably associated with one of the larger channel systems in the lower Kada Hadar Member[25], which contain large root casts and tree trunks[24] (Supplementary Note 5). Channels and crevasse-splays are usually heavily vegetated along their banks, and together these data show that trees were common at Hadar.

Table 2 | Free fall velocity and energy from tree nest height

Chimpanzee tree nest heights (*n*)*	Metres	Velocity $m\,s^{-1}$†	Velocity $km\,h^{-1}$	Lucy's PE (kJ)‡ Mean	Lucy's PE (kJ)‡ Lower interval	Lucy's PE (kJ)‡ Upper interval
Savannah mean (10)	13.71	16.40	59.05	3.50	2.31	5.27
Savannah mean of minimum (7)	4.67	9.57	34.45	1.19	0.79	1.79
Savannah mean of maximum (7)	35.83	26.51	95.45	9.14	6.05	13.78
Savannah maximum	47.80	30.62	110.25	12.19	8.07	18.38
Forest mean (31)	13.08	16.02	57.67	3.34	2.21	5.03
Forest mean of minimum (17)	3.09	7.79	28.05	0.79	0.52	1.19
Forest mean of maximum (22)	34.52	26.02	93.69	8.80	5.82	13.27
Forest maximum	50.00	31.32	112.76	12.75	8.44	19.23

*Study site tree nest heights from ref. 27. Maximum and minimum heights not reported for all sites.
†Velocity = $\sqrt{2 \times \text{height (m)} \times 9.81\,\text{m s}^{-2}}$.
‡Potential energy (PE) (kJ) = mass (kg) × height (m) × 9.81 m s^{-2}/1,000. Lucy's body mass estimated as 26 kg (17.2–39.2 kg lower–upper interval) from ref. 31.

If Lucy sought out trees for food and nightly nesting sites, other similar-sized primates, such as chimpanzees, offer important information about the heights to which she might have climbed. Chimpanzees forage widely through the canopy, and at Kibale log a daily average of 3–5 climbing bouts to heights of 95–135 m in fruit trees[26]. The typical heights of chimpanzees' sleeping nests in savanna habitat study sites range from means of 8.3 to 21.0 m (mean 13.71 m, $n = 10$) whereas in forested habitat study sites the means range from 7.1 to 23.2 m (mean 13.08 m, $n = 31$) (Table 2)[27]. If a building storey is taken to be about 3 m, these mean heights equate to four- to five-storey buildings, with the range of means varying from nearly three to seven stories, and maximum heights of about 16 stories; these are considerable heights.

Falls from height

Chimpanzees and some modern humans move and forage in trees and sometimes experience skeletal trauma and death from falls (Supplementary Note 6). Even though chimpanzee foraging heights frequently exceed sleeping nest heights[28], nest data offer a conservative approach for assessing whether skeletal trauma and death are likely to result from a fall at these heights. Average velocities (Table 2) for unimpeded free falls from nest height means reach nearly 60 km h^{-1}, and the associated energies[29] (Table 2) are within the range known to cause fatal impacts in humans[30], with the generally lower energies estimated for Lucy resulting from her lower body mass[31] (Supplementary Note 7). Impacts from these heights often produce a wide range of concomitant fractures in humans[15–18,30] similar to those preserved in Lucy's skeleton. Such falls usually severely damage internal organs because they too decelerate upon impact and can be penetrated by broken bones, damaged by compression between the sternum and spine, and experience a 'hydraulic ram effect' in which abdominal organs are thrust upwards to produce cardiac damage[16].

Scenario for Lucy's perimortem fractures

The pattern of compressive and hinge fractures, palaeohabitat reconstruction, sedimentology of the discovery site, and consistency

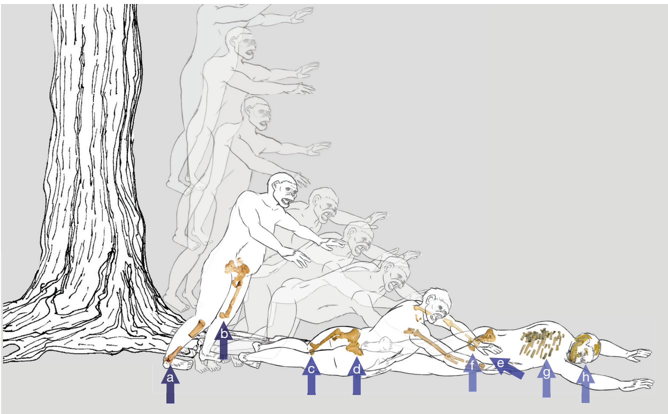

Figure 2 | Reconstruction of Lucy's vertical deceleration event. We hypothesize that Lucy fell from a tall tree, landing feet-first and twisting to the right, with arrows indicating the sequence and types of fractures. **a**, Pilon fracture, tibial plateau fracture, and spiral shaft fracture of right tibia. **b**, The impact of hyperextended left knee drove the distal femoral epiphysis into the distal shaft, and fractured the femoral neck and possibly the acetabulum, sacrum, and lumbar vertebra. **c**, The impact of the knee drove the patella into the centre anterodistal surface of the femoral shaft. **d**, Impact on the right hip drove the right innominate into the sacrum, and the sacrum into the left innominate, dislocating and fracturing the sacrum and left innominate, and elevating the retroauricular surface. **e**, Lucy was still conscious when she stretched out her arms in an attempt to break her fall and fractured both proximal humeri, the right more severely than the left with spiral fracture near the midshaft, a Colles' (or Smith's) fracture of the right radius, and perhaps other fractures of the radii and ulnae. The impact depressed and retracted the right scapula, which depressed the clavicle into the first rib, fracturing both. **f**, Frontal impact fractured the left pubis and drove a portion of the anterior inferior pubic ramus posterolaterally, and a branch or rock possibly created the puncture mark on the pubis. **g**, The impact of the thorax fractured many ribs and possibly some thoracic vertebrae. **h**, The impact of the skull, slightly left of centre, created a tripartite guardsman fracture of the mandible and cranial fractures. See Supplementary Methods and Supplementary Video 4.

with clinical cases lead us to propose that the following scenario is the most likely of the various possible injury mechanisms: Lucy fell out of a tall tree at or in proximity to the distributary crevasse splay channel where her remains were found. Given the severity of the fractures, it is likely that the impact occurred on a hard surface, perhaps the dry bed of the channel itself, which would represent a near-zero stopping distance, thereby maximizing the transfer of energy produced by the fall. The body appears to have experienced minimal transport and rapid burial after death in order to retain the relative positions of the small fractured bone fragments. The location and severity of the fractures suggest that impact progressed from the feet and legs to the hip, arms, thorax, and head (Fig. 2 and Supplementary Video 4). Concomitant fractures and organ damage are witnessed in the most severe clinical cases and together contribute to the death of the victim[15–18]. Although the fractures in Lucy's humeri provide evidence that she was conscious when she stretched out her arms in an attempt to break her fall, the severity of the numerous compressive fractures and presumed organ damage suggest that death followed swiftly.

Discussion

Although most hominin fossils are fragmentary and broken because of a complex post-mortem history, skeletal elements sometimes preserve evidence of antemortem or perimortem fractures and injuries[5–7]. When examining fossil taxa, such as *Australopithecus afarensis*[3,19], that appear to have practiced both terrestrial and arboreal locomotion, we suggest that the adaptations that facilitated bipedal terrestrial locomotion compromised the ability of individuals to climb safely and efficiently in the trees; this combination of features may have predisposed these taxa to more frequent falls from height. Close inspection of other fossil specimens for antemortem or perimortem fractures (Supplementary Note 8) has the potential to offer important information about their lifestyles through an understanding of the trauma that they suffered and the mechanisms by which they died.

Online Content Methods, along with any additional Extended Data display items and Source Data, are available in the online version of the paper; references unique to these sections appear only in the online paper.

Received 21 April; accepted 25 July 2016.
Published online 29 August 2016.

1. Johanson, D. C. & Taieb, M. Plio–Pleistocene hominid discoveries in Hadar, Ethiopia. *Nature* **260,** 293–297 (1976).
2. Johanson, D. C. *et al.* New partial skeleton of *Homo habilis* from Olduvai Gorge, Tanzania. *Nature* **327,** 205–209 (1987).
3. Alemseged, Z. *et al.* A juvenile early hominin skeleton from Dikika, Ethiopia. *Nature* **443,** 296–301 (2006).
4. White, T. D. *et al. Ardipithecus ramidus* and the paleobiology of early hominids. *Science* **326,** 75–86 (2009).
5. Haile-Selassie, Y. *et al.* An early *Australopithecus afarensis* postcranium from Woranso-Mille, Ethiopia. *Proc. Natl Acad. Sci. USA* **107,** 12121–12126 (2010).
6. Walker, A. & Shipman, P. *The Wisdom of the Bones* (Knopf, 1996).
7. L'Abbé, E. N. *et al.* Evidence of fatal skeletal injuries on Malapa Hominins 1 and 2. *Sci. Rep.* **5,** 15120 (2015).
8. Walter, R. C. Age of Lucy and the first family: single-crystal $^{40}Ar/^{39}Ar$ dating of the Denen Dora and lower Kada Hadar members of the Hadar Formation, Ethiopia. *Geology* **22,** 6–10 (1994).
9. Johanson, D. C. *et al.* Morphology of the Pliocene partial hominid skeleton (A.L. 288-1) from the Hadar Formation, Ethiopia. *Am. J. Phys. Anthropol.* **57,** 403–451 (1982).
10. Armitage, B. M. *et al.* Mapping of scapular fractures with three-dimensional computed tomography. *J. Bone Joint Surg. Am.* **91,** 2222–2228 (2009).
11. Neer, C. S., II. Displaced proximal humeral fractures. I. Classification and evaluation. *J. Bone Joint Surg. Am.* **52,** 1077–1089 (1970).
12. Edelson, G., Kelly, I., Vigder, F. & Reis, N. D. A three-dimensional classification for fractures of the proximal humerus. *J. Bone Joint Surg. Br.* **86,** 413–425 (2004).
13. Twiss, T. in *Proximal Humerus Fractures: Evaluation and Management* (eds Crosby, L. A. & Neviaser, R. J.) 23–41 (Springer, 2015).
14. Jaiswal, A. *et al.* Bilateral traumatic proximal humerus fractures managed by open reduction and internal fixation with locked plates. *Chin. J. Traumatol.* **16,** 379–381 (2013).
15. Snyder, R. G. Human tolerances of extreme impacts in free fall. *Aerosp. Med.* **34,** 695–709 (1963).
16. Goonetilleke, U. K. D. A. Injuries caused by falls from heights. *Med. Sci. Law* **20,** 262–275 (1980).
17. Papadopoulos, I. N. *et al.* Patients with pelvic fractures due to falls: A paradigm that contributed to autopsy-based audit of trauma in Greece. *J. Trauma Manag. Outcomes* **5,** 2–15 (2011).
18. Auñón-Martín, I. *et al.* Correlation between pattern and mechanism of injury of free fall. *Strateg. Trauma Limb Reconstr.* **7,** 141–145 (2012).
19. Stern, J. T. Climbing to the top: a personal memoir of *Australopithecus afarensis*. *Evol. Anthropol.* **9,** 113–133 (2000).
20. Stewart, F. A. & Pruetz, J. D. Do chimpanzee nests serve an anti-predatory function? *Am. J. Primatol.* **75,** 593–604 (2013).
21. Reed, K. E. Paleoecological patterns at the Hadar hominin site, Afar Regional State, Ethiopia. *J. Hum. Evol.* **54,** 743–768 (2008).
22. Bonnefille, R., Potts, R., Chalié, F., Jolly, D. & Peyron, O. High-resolution vegetation and climate change associated with Pliocene *Australopithecus afarensis. Proc. Natl Acad. Sci. USA* **101,** 12125–12129 (2004).
23. Aronson, J. L., Hailemichael, M. & Savin, S. M. Hominid environments at Hadar from paleosol studies in a framework of Ethiopian climate change. *J. Hum. Evol.* **55,** 532–550 (2008).
24. Yemane, T. *Stratigraphy and sedimentology of the Hadar Formation*. PhD thesis, Iowa State Univ. (1997).
25. Campisano, C. J. & Feibel, C. S. Depositional environments and stratigraphic summary of the Pliocene Hadar Formation at Hadar, Afar Depression, Ethiopia. *GSA Special Papers* **446,** 179–201 (2008).
26. Pontzer, H. & Wrangham, R. W. Climbing and the daily energy cost of locomotion in wild chimpanzees: implications for hominoid locomotor evolution. *J. Hum. Evol.* **46,** 315–333 (2004).
27. Hernandez-Aguilar, R. A., Moore, J. & Stanford, C. B. Chimpanzee nesting patterns in savanna habitat: environmental influences and preferences. *Am. J. Primatol.* **75,** 979–994 (2013).
28. Doran, D. M. Sex differences in adult chimpanzee positional behavior: the influence of body size on locomotion and posture. *Am. J. Phys. Anthropol.* **91,** 99–115 (1993).
29. Warner, K. G. & Demling, R. H. The pathophysiology of free-fall injury. *Ann. Emerg. Med.* **15,** 1088–1093 (1986).

30. Weilemann, Y., Thali, M. J., Kneubuehl, B. P. & Bolliger, S. A. Correlation between skeletal trauma and energy in falls from great height detected by post-mortem multislice computed tomography (MSCT). *Forensic Sci. Int.* **180,** 81–85 (2008).
31. Grabowski, M., Hatala, K. G., Jungers, W. L. & Richmond, B. G. Body mass estimates of hominin fossils and the evolution of human body size. *J. Hum. Evol.* **85,** 75–93 (2015).

Supplementary Information is available in the online version of the paper.

Acknowledgements We thank the Authority for Research and Conservation of Cultural Heritage and the National Museum of Ethiopia of the Ministry of Tourism and Culture for permission to scan, study, and photograph Lucy; A. Admassu, K. Ayele, J. A. Bartsch, Y. Beyene, Y. Desta, R. Diehl, R. Flores, R. Harvey, G. Kebede, R. Lariviere, J. H. Mariam, S. M. Miller, L. Rebori, B. Roberts, J. Ten Barge, J. M. Sanchez, D. Slesnick, D. Van Tuerenhout, S. Wilson, M. Woldehan, and M. Yilma for facilitating and assisting with the scanning; T. Getachew and M. Endalamaw for assisting with the photography, and S. Mattox for many of the photographs; V. A. Lopez and S. Robertson for Fig. 2; C. Bramblett, B. Brown, C. Campisano, J. G. Fleagle, T. Helpenstell and colleagues at Olympia Orthopaedic Associates, A. L. Kappelman, J. A. Kappelman, S. Khosropour, H. Pontzer, D. Reed, C. B. Ruff, J. T. Stern Jr, and S. C. Ward for discussions; the Paleoanthropology Laboratory Fund, College of Liberal Arts UT Austin, and Houston Museum of Natural Science for financial and logistical support; and Owen-Coates Fund of the Geology Foundation of UT Austin for publication costs. The University of Texas High-Resolution X-ray CT Facility was supported by US National Science Foundation grants EAR-0646848, EAR-0948842, and EAR-1258878.

Author Contributions J.K. conceived the project; J.K., R.A.K., S.P., L.T. and M.F. collected data; W.A., M.W.C., J.K. and A.W. completed the 3D reconstruction and video of the right humerus; and J.A.M. completed the 3D videos of the mandible. J.K. wrote the paper with comments from all authors.

Author Information Reprints and permissions information is available at www.nature.com/reprints. The authors declare no competing financial interests. Readers are welcome to comment on the online version of the paper. Correspondence and requests for materials should be addressed to J.K. (jkappelman@austin.utexas.edu).

Reviewer Information *Nature* thanks S. Black, W. Jungers and the other anonymous reviewer(s) for their contribution to the peer review of this work.

METHODS

CT scanning of A.L. 288-1. All scans were performed at the University of Texas High-Resolution X-ray CT Facility with procedures described in ref. 32, using a FeinFocus FXE 225 kV X-ray source and image intensifier detector captured by a 1024×1024 CCD camera. Samples were held in place by custom foam mounts within Plexiglas containers, and the X-ray signal was calibrated using empty containers. X-ray settings were 180 kV and 0.175–0.180 mA, with an estimated focal spot size of $\sim$40 μm, and no beam filtration was used. Scanning parameters were optimized for each piece based on size, and in some cases multiple pieces were scanned simultaneously. During each turntable rotation, 1,200 views (projections) were acquired to obtain raw data for 25 slices. Raw data were reconstructed as 16-bit TIFF images. Beam hardening corrections were performed during reconstruction using polynomial linearization[33], with coefficients selected independently for each scan owing to variations in mineralization. Ring artefacts were corrected either pre- or post-reconstruction[34]. Reconstruction scaling of CT numbers was reduced for pieces that had highly attenuating mineralization, probably oxides or sulfides, to avoid information loss from voxel saturation. See Extended Data Table 1 for acquisition parameters, data voxel dimensions, and scaling and artefact processing parameters.

3D reconstruction. Data volumes were loaded into Avizo (FEI) in order to produce the 3D element and segment the individual bone fragments along fracture planes, with each fragment saved as an .stl file. These files were imported into Autodesk's Maya and were repositioned, reoriented, and aligned along fracture planes to reconstruct the element. A 3D scan of the left proximal humerus mirrored as a right was used as an approximate template for reconstructing the right proximal humerus. The keyframe function in Maya was used to move each individual fragment from its reconstructed 'before' position to its discovery 'after' position in order to recreate the progression of the impact injury (Extended Data Figs 1, 2 and Supplementary Video 1).

Digital photography. Digital photographs of the original fossils and replica casts were taken against a black felt or velvet background and imported into Adobe Photoshop C5.1 Extended at full resolution. The element was isolated with the lasso tool and cut and pasted onto a solid colour background, with stereo views composed of elements in different layers. Tracings of the fractures were made in separate layers with Photoshop's pencil or lasso and fill tools.

32. Ketcham, R. A. & Carlson, W. D. Acquisition, optimization and interpretation of X-ray computed tomographic imagery: applications to the geosciences. *Comput. Geosci.* **27,** 381–400 (2001).
33. Herman, G. T. Correction for beam hardening in computed tomography. *Phys. Med. Biol.* **24,** 81–106 (1979).
34. Ketcham, R. A. New algorithms for ring artifact removal. *Proc. SPIE* **6318,** 10.1117/12.680939 (2006).

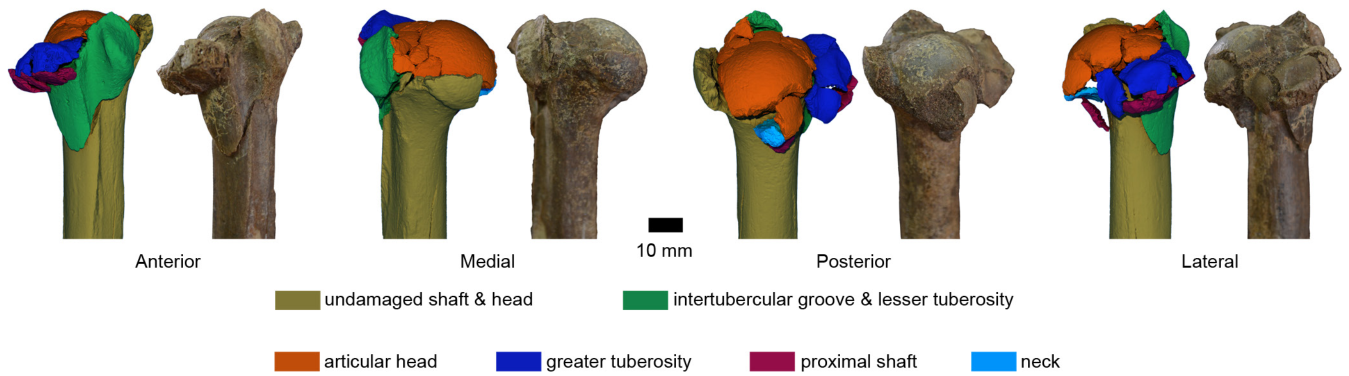

Extended Data Figure 1 | Right humerus (A.L. 288-1m) CT segmentation compared with photographs of fossil. Right proximal humerus (A.L. 288-1m) illustrating the fractured fragments segmented from the CT scans compared with photographs of fossil. Nearly 30 fractured bone and articular head fragments and slivers were isolated by segmentation. Some small fragments remain embedded within the sediment on the posterior aspect of the head. One large fragment was avulsed off of the posteroinferior aspect of the articular head and not recovered. Scale bar, 10 mm. See Methods, Extended Data Fig. 2 and Supplementary Note 1 for a full description; also see Supplementary Video 1.

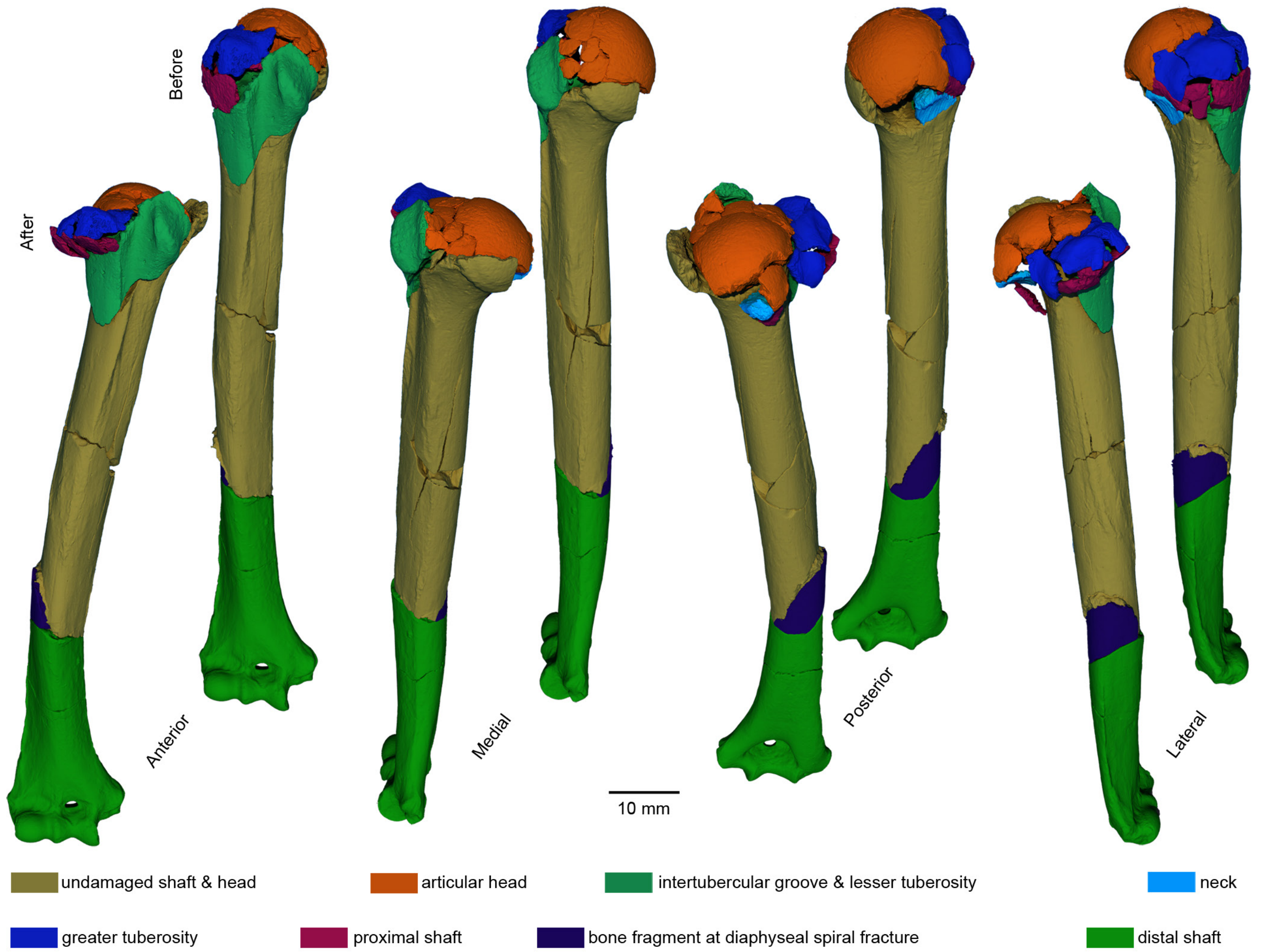

Extended Data Figure 2 | Right humerus (A.L. 288-1m) CT segmentation with 'before' reconstruction and 'after' discovery state. Right proximal humerus (A.L. 288-1m) illustrating the head and diaphyseal shaft fragments segmented from the CT scans. The before image presents a reconstruction of the crushed proximal portion of the head that also straightens the spiral fracture at the diaphysis, and the after image shows the condition of the fossil in its discovery state. The impact compressed the proximal humerus against the glenoid of the scapula, with the glenoid acting as an anvil, which in turn fractured and shattered the components of the proximal humerus including the articular head, greater and lesser tuberosities, and shaft. Each pair of before and after images depicts the distal portion of the shaft in the same position and illustrates how the proximal portion of the head and shaft were angled in a posteromedial direction by the fracture. In some pairs of images the proximal end of the humerus is angled slightly towards the viewer to show a greater percentage of the head. Scale bar, 10 mm (approximate because of the differences in perspective). See Methods, Fig. 1, Extended Data Fig. 1 and Supplementary Note 1 for a full description; also see Supplementary Video 1.

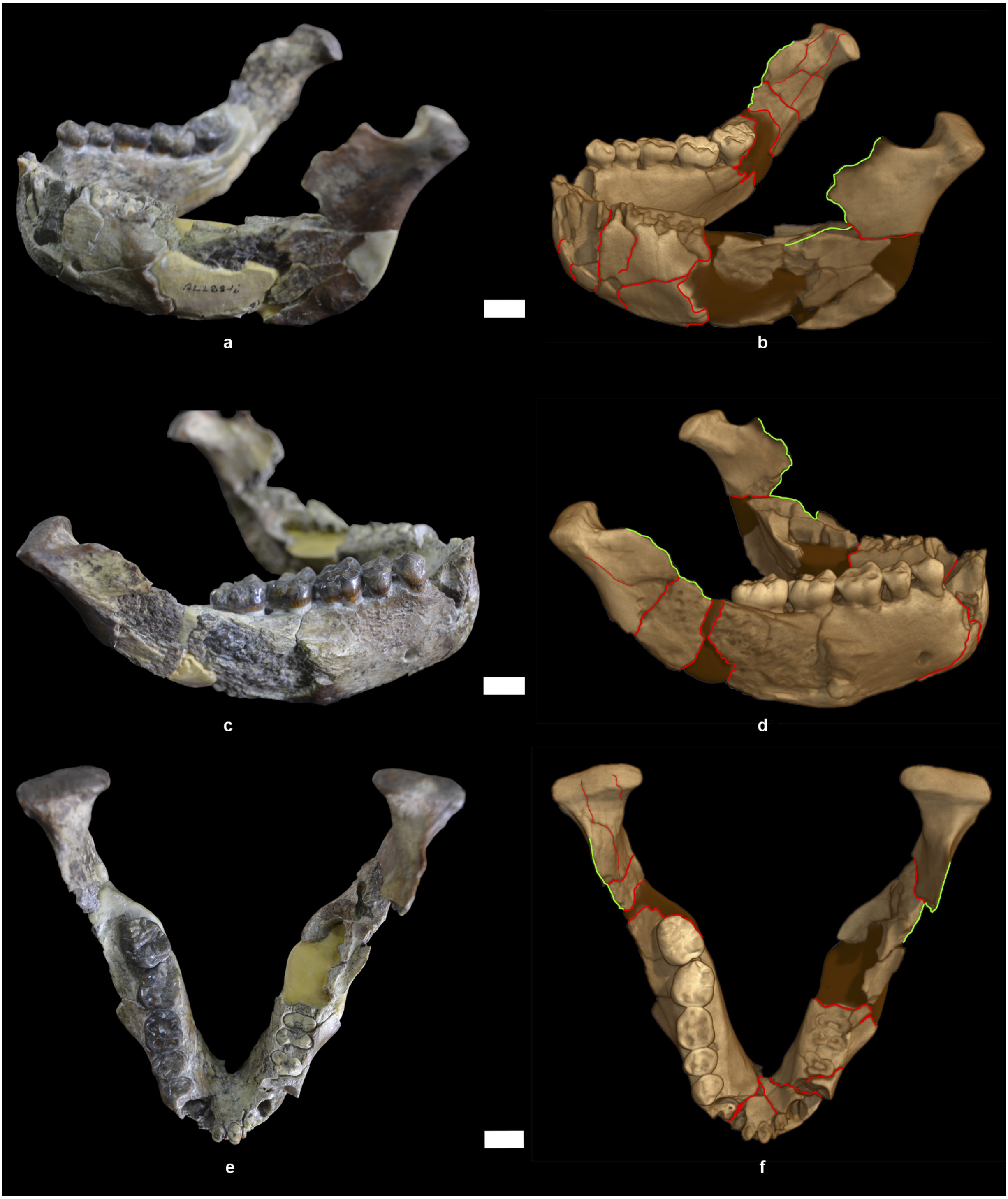

Extended Data Figure 3 | Mandible (A.L. 288-1i, -1j and -1k) photographs and CT scan. A comparison of photographs with CT scan of mandible (A.L. 288-1i, -1j and -1k) illustrating in red the major fractures across the parasymphyseal region, left body, and left (A.L. 288-1j) and right (A.L. 288-1k) subcondylar regions; and in green the fractures across the edges of the coronoid processes. The condyles were discovered and catalogued as separate specimens, and there is a set of closed fractures through the right condyle. Binding materials used in the reconstruction of the mandible are seen in yellow in the photographs, and as smooth dark brown in the CT scans. Note the generally tight contacts between adjacent bone fragments. Right p3–m3 teeth are complete whereas the anterior dentition and the teeth on the left side are fractured along the base of their crowns or are missing. This fracture pattern is typical of a tripartite guardsman fracture with fractures at parasymphysis and bilateral fractures in the subcondylar region. **a**, **b**, Left anterolateral view; **c**, **d**, right anterolateral view; **e**, **f**, superior view. Scale bars, approximately 10 mm because of angled views. See Supplementary Note 1 for a full description; also see Supplementary Videos 2, 3.

Extended Data Figure 4 | Mandible (A.L. 288-1i, -1j and -1k) CT scan. CT scan of mandible (A.L. 288-1i, -1j and -1k) illustrating in red the major fractures across the parasymphyseal region, left body, and left (A.L. 288-1j) and right (A.L. 288-1k) subcondylar regions. The coronoid processes are missing and their fractured edges outlined in green. This fracture pattern is typical of a tripartite guardsman fracture with fractures at parasymphysis and bilateral fractures in the subcondylar region. **a**, Anterior view; **b**, posterior view; **c**, superior view; **d**, inferior view. **e**–**g**, Anterior views of coronal slices: **e**, slice through the centre of canine alveolae that shows the major parasymphyseal fractures; **f**, slice at mesial edge of m3; and **g**, slice through mesial edge of coronoid process that shows the position of the right and left subcondylar fractures. Scale bar, 10 mm. See Supplementary Note 1 for a full description; also see Supplementary Videos 2, 3.

Extended Data Table 1 | Scan parameters for A.L. 288-1

Specimen Number	Element	kV	mA	Focal spot size (mm)	Views	Slices per rotation	Seconds per view	SOD (mm)	Spacing slice (mm)	Spacing pixel (mm)	Reconstruction offset	Reconstruction scale	BHC parameters	Ring processing
A. L. 288-1m	Right distal humerus	180	0.175	0.04	1200	25	0.400 (slices 1-675); 0.133 (slices 676-1408)	192	0.0670	0.0615	5000	3000	[0, 0.6, 0.05, 0.05]	post
A. L. 288-1m	Right proximal humerus	180	0.175	0.04	1200	25	0.533 (slices 1-650); 0.133 (slices 651-2982)	144	0.0502	0.0459	5000	500	[0, 0.75, 0.05, 0.05]	pre
A. L. 288-1r	Left proximal humerus	180	0.175	0.04	1200	25	0.533 (slices 1-650); 0.133 (slices 651-2775)	114	0.0398	0.0361	5000	3000	[0, 0.7, 0.15]	post
A. L. 288-1s	Left distal humerus	180	0.175	0.04	1200	25	0.400 (slices 1-675); 0.133 (slices 676-1408)	192	0.0670	0.0615	5000	3000	[0, 0.6, 0.05, 0.05]	post
A. L. 288-1l	Right scapula	220	0.4	0.11	1200	15	0.533 (slices 1-210)	303	0.1057	0.0977	5000	3000	[0, 0.65, 0, 0.1]	post
A. L. 288-1i, -1j, -1k	Mandible	220	0.4	0.11	1800	15	0.2 (slice 1-801)	370	0.1189	0.1290	5000	5000	[0, 0.5, 0.01, 0.1]	pre